# UC Irvine

## UC Irvine Previously Published Works

## Title

Spectroscopy enhances the information content of optical mammography

## Permalink

https://escholarship.org/uc/item/8bq2x4zt

## Journal

Journal of Biomedical Optics, 7(1)

## ISSN

1083-3668

## Authors

Cerussi, AE
Jakubowski, D
Shah, N
et al.

## Publication Date

2002

## DOI

10.1117/1.1427050

## Copyright Information

Peer reviewed

# Spectroscopy enhances the information content of optical mammography

**A. E. Cerussi**
**D. Jakubowski**
**N. Shah**
**F. Bevilacqua**
**R. Lanning**
University of California, Irvine
Beckman Laser Institute and Medical Clinic
1002 Health Sciences Rd.
Irvine, California 92612

**A. J. Berger**
University of Rochester
Institute of Optics
Wilmot 418
Rochester, New York 14627

**D. Hsiang**
**J. Butler**
University of California, Irvine Medical Center
Department of Oncological Surgery
101 The City Dr.
Orange, California 92868

**R. F. Holcombe**
University of California, Irvine Medical Center
Division of Hematology/Oncology
101 The City Dr.
Orange, California 92868

**B. J. Tromberg**
University of California, Irvine
Beckman Laser Institute and Medical Clinic
1002 Health Sciences Rd.
Irvine, Californai 92612

**Abstract.** Near-infrared (NIR) diffuse optical spectroscopy and imaging may enhance existing technologies for breast cancer screening, diagnosis, and treatment. NIR techniques are based on quantitative measurements of functional contrast between healthy and diseased tissue. In this study we measured the spectral dependence of tissue absorption ($\mu_a$) and reduced scattering ($\mu_s'$) in the breasts of 30 healthy women and one woman with a fibroadenoma using a seven-wavelength frequency-domain photon migration probe. Subjects included pre- and postmenopausal women between the ages of 18 and 64. Multi-spectral measurements were used along with a four-component fit to determine the concentrations of de-oxy and oxy-hemoglobin, water and lipids in breast. The scattering spectral shape was also quantified. Our measurements demonstrate that the measured concentrations of NIR analytes correlate well with known breast physiology. Although the tissue scattering at a single wavelength was found to have little value as a functional parameter, the dependence of the scattering on wavelength provided key insights into breast composition and physiology. Lipids and scattering spectra in the breast were found to increase and decrease, respectively, with increasing body mass index. Simple calculations are also provided to demonstrate potential penalties from ignoring the contributions of water and lipids in breast measurements. Finally, water is shown to be a possible indicator for detecting a fibroadenoma, whereas the hemoglobin saturation was found to be a poor indicator. Multi-spectral measurements, compared to measurements restricted to one or two wavelengths, provide additional information that may be useful in managing breast disease. © 2002 Society of Photo-Optical Instrumentation Engineers.
[DOI: 10.1117/1.1427050]

## 1 Introduction

### 1.1 Role of Optics

Near-infrared (NIR) photon migration spectroscopy provides quantitative functional information from breast tissue that cannot be obtained by conventional radiologic techniques. NIR techniques are sensitive to several important physiological components in tissue such as hemoglobin and water. In the clinical management of breast disease, such functional information suggests a variety of potential medical applications: therapeutic monitoring (angiogenesis, chemotherapy), supplemental lesion characterization (benign versus malignant), and risk assessment (origins of breast density). A noninvasive optical imaging technique that provides unique, quantitative physiological information can greatly enhance current screening and diagnostic monitoring for the breast. Emerging techniques for the breast such as magnetic resonance imaging and positron emission tomography have shown promise in providing functional images. However, these techniques are costly,

cumbersome, and rely upon the use of contrast agents. On the contrary, NIR techniques may be used with either endogenous or exogenous contrast, and can be fashioned into inexpensive and portable systems.

### 1.2 History of Early Breast Optics

Although white-light transillumination was introduced into medicine in the early 1800's, it was not until 1929 that the technique was formally applied as a tool to visualize the shadows cast by breast lesions.[1] Carlsen introduced spectral breast imaging in 1980 by restricting the light source of a medical transillumination imager to red and NIR bands.[2] Images consisted of the ratios between red and NIR light traveling through the breast. Throughout the 1980's there were a variety of clinical trials attempting to compare various transillumination/diaphanography instruments with mammography as a screening tool; a potpourri of conflicting clinical conclusions was the result. (The literature is often vague in distinguishing transillumination/lightscanning from diaphan-

Address all correspondence to Dr. Bruce J. Tromberg. Tel: 949-824-8705; Fax: 949-824-8413; E-mail: tromberg@bli.uci.edu

ography. Typically, transillumination refers to white-light illumination, whereas diaphanography refers to red and NIR illumination.) Some studies, most notably those of Bartrum and Crow,[3] Wallberg et al.,[4] and Budred et al.,[5] have shown very favorable results comparing optical and radiological devices as screening tools. Other studies, most notably by Drexler, Davis, and Schofield,[6] Monsees, Destouet, and Gersell,[7] and Alveryd et al.[8] have shown quite the opposite. Such studies, and in particular the one by Alveryd et al., dissuaded further development of the technique, as evidenced by the refusal of insurance companies to offer coverage for optical breast exams.

Many reasons have been cited to explain the failures of these early optical methods to detect and to classify breast lesions. Some cited study-dependent issues such as poor operator experience and inadequate statistical analysis. More seriously, there were physical limitations such as inadequate light penetration, poor dynamic range, inadequate spatial resolution, uncorrected geometrical and boundary effects, and tissue scattering. Clinically, the physical limitations of diaphanography manifested as very high false positive rates as well as low true positive rates. Although the highly scattering nature of tissues could never allow resolution comparable to radiography, the early stages of optical breast exams relied upon direct visualization of the lesion.[9] Although direct visualization of lesion anatomy is difficult, if not impossible with visible/NIR optics, *spectroscopic* visualization of tissue function is an entirely different matter.

### 1.3 Importance of Spectroscopy

Recent developments in functional methods such as diffuse optical spectroscopy (DOS) and diffuse optical tomography offer distinct advantages over traditional diaphanography. DOS may be used to quantify tissue biochemical composition. For example, dual-wavelength spectroscopy has been widely used to determine the absorption coefficient ($\mu_a$) and hence the concentrations of reduced hemoglobin (Hb-R) and oxygenated hemoglobin (Hb-O$_2$) in tissue.[10] However, NIR light absorption in breast is due to more than just hemoglobin.[11] Although water and lipid are weak NIR absorbers, their high abundance in breast tissue relative to hemoglobin translates into significant absorption, particularly in the 900–1000 nm range.[11–13] Moreover, the balance of water and lipid in the breast depend on factors such as age and hormonal status. A complete physiological picture of breast requires knowledge of this balance.[14,15] Restricting measurements to only two wavelengths to measure Hb-R and Hb-O$_2$ compromises both the accuracy and completeness of tissue characterization.

The spectral dependence of tissue scattering in its own right may also contain important functional information. Tissues scatter NIR light very strongly, such that the separation of reduced scattering ($\mu_s'$) from absorption is critical for extracting the true absorption spectrum of the tissue. Although the distribution of NIR scattering centers in tissue is not well understood, multi-spectral NIR measurements of $\mu_s'$ have shown a relationship between scattering and wavelength.[16,17] Spectral measurements of tissue scattering may provide information about the types of scattering centers found in a given region of tissue, and in turn provide information about tissue cellularity,[18] composition,[19] and disease state.[20]

Early studies have shown that red and NIR light absorption in breast is highly sensitive to hemoglobin.[21,22] However, the presence of blood alone is not sufficient criteria for the diagnosis of cancer, a weakness that probably contributed to the high false positive rate of diaphanography. Neglecting scattering diminishes contrast even further. Additional information about metabolism and water content may be the key to avoiding poor sensitivity and specificity. Limiting measurements to a few wavelengths greatly limits sensitivity, and does not take advantage of the full capabilities of optical spectroscopy.

### 1.4 Modern Breast Optics

Continuous wave, fixed distance methods (i.e., source detector separation) measure light attenuation. Recent advances in the understanding of the propagation of pulsed light in multiply scattering media such as tissues have provided methods to separate $\mu_a$ and $\mu_s'$ in both the time[23] and frequency domains.[24] Scattering values for breast lesions have been measured *in vivo* to be both lower[19,25] and higher[19] than normal tissue. The nature of these differences is not clear.

Prototype commercial instruments have implemented raw intensity[26,27] because it is simple and inexpensive. One commercial device used a frequency-domain correction for breast thickness, which dramatically improved their results.[28] Modern time-resolved and frequency-domain NIR spectroscopy can monitor tissue physiological activity such as hemoglobin saturation and thereby distinguish between diseased and healthy tissue upon a functional basis. Such techniques have quantified the metabolism of small palpable lesions *in vivo* in humans, thus demonstrating the feasibility of NIR methods for breast cancer screening and detection.[29–32] Simultaneous acquisition of multi-spectral information is also being considered.[33]

In recent years NIR tissue spectroscopy has been used to study healthy breast tissue and changes that occur with age, hormone use, and other factors. Kang et al. apparently supplied one of the first *in vivo* optical measurements of breast tissue.[34] Suzuki et al. performed time-resolved spectroscopy at a single wavelength to detect changes in optical properties as a factor of age,[35] menopause, and body mass index (BMI).[36] Heusmann, Kölzer, and Mitic measured the effects of water in normal breast tissues using incomplete published scattering curves.[37] Quaresima, Matcher, and Ferrari measured the intra- and inter-subject variability of the optical properties of healthy women using second-derivative spectroscopy, again using published scattering data.[12] Cubeddu et al. studied physiological changes in breast optical properties during the five phases of the menstrual cycle using a time-resolved, multi-spectral approach.[13]

### 1.5 Scope of This Work

We believe that the key to the success of optical methods in breast lies in the spectroscopic content of the optical signals. Common procedure has been to compare the optical properties of diseased tissue to ''normal'' breast tissue. Normal breast tissue is a vague concept, given the frequency and magnitude of changes that occur over a variety of time scales. Despite this fact, there is a scarce amount of information available on the optical signature of nondiseased breast tissue. The physiology of healthy breast tissue is complex, influenced

by multiple internal and external factors such as menstrual cycle, menopause, exogenous hormones, lactation and pregnancy. Some of these changes have been monitored qualitatively by mammography and magnetic resonance imaging.[38–40]

This paper represents a continuing effort to quantify the composition and function of breast tissue using NIR spectroscopy. All of the 30 healthy subjects we studied had not manifested any forms of breast disease at the time of the measurement. We have shown that both absorption and scattering spectral signatures provide important clues about the functional state of breast tissue. Such information may prove critical to the advancement of modern biomedical optics in the breast, and improve upon measurements of intensity alone.[26] In addition, we provide broadband spectroscopic measurement of a fibroadenoma *in vivo*, demonstrating the enormous contrast available to multi-spectral optical measurements.

## 2 Materials and Methods

### 2.1 General Approach

The dependence of the chromophore concentration on the absorbance of light is $AB = \epsilon[c]l$, where $\epsilon$ is the molar extinction coefficient ($M^{-1} cm^{-1}$), $[c]$ is the concentration of chromophore $c$ ($M L^{-1}$), and $l$ is the photon path length (cm). The path length $l$ is increased by scattering and is not known *a priori*. Time-resolved and phase-sensitive methods that measure the time course of photons (or equivalently, $l$) have been used to separate the effects of absorption and scattering on the attenuation of light.[23,24] The absorption coefficients translate into tissue chromophore concentrations using the equation

$$\mu_a = 2.303\epsilon[c]. \tag{1}$$

The factor of 2.303 originates from the base conversion between the logarithm for absorbance and the natural logarithm for $\mu_a$.

### 2.2 Measurement of Absorption and Scattering

The theory of frequency-domain photon migration (FDPM) is based upon the formation, the propagation, and the characterization of density waves of individual photons inside a multiply scattering medium. The technical aspects of this theory have been discussed in the literature.[24,41] The behavior of these photon density waves (PDW) is mediated by two wave characteristics, [frequency, $f$ (MHz) and distance traveled, $r$ (mm)], and two media characteristics ($\mu_a$ and $\mu_s'$). The modulation frequency is the rate at which a light source is turned on and off and has nothing to do with the energy or color of the light.

Our typical experimental configuration is to measure the real and imaginary parts of this wave at a fixed distance between light source and optical detector over a range of source modulation frequencies, ranging from 50 to 1000 MHz. For the purposes of physical intuition, we may translate these real and imaginary parts of the photon density, $U$ (photons per cubic mm), into the amplitude ($\psi$) and phase ($\phi$) of the photon density wave

$$\psi = \sqrt{\text{Re}(U)^2 + \text{Im}(U)^2}, \tag{2}$$

$$\phi = \arctan\left(\frac{\text{Im}(U)}{\text{Re}(U)}\right). \tag{3}$$

The frequency-domain expression for $U$ is given by the $P_1$ approximation to the Boltzmann transport equation.[42,43] We selected the $P_1$ model over the standard diffusion model because the $P_1$ approximation has a more accurate frequency response at higher modulation frequencies and introduces little additional complexity. The model geometry used in this paper was a semi-infinite medium, where the solution was obtained by using the method of images for the infinite medium solution along with an extrapolated boundary.[23] The index of refraction mismatch was taken into account using the empirical polynomial fit of Groenhuis, Ferwerda, and Ten Bosch[44] and assuming a tissue index of refraction of 1.4.[45] We assume that both $\mu_a$ and $\mu_s'$ represent a macroscopically homogeneous average value of the tissue that is sampled by the light.

### 2.3 Fitting Considerations

By fitting instrument-corrected data to the appropriate physical model, we can recover $\mu_a$ independently from $\mu_s'$ for the tissue. We typically fit data from 100 to 700 MHz while keeping $r$ fixed at 22 mm in order to recover $\mu_a$ and $\mu_s'$. A Levenberg-Marquardt minimization algorithm was adapted to fit simultaneously both the real and imaginary (i.e., phase and amplitude analogs) parts of the signal by minimizing a $\chi^2$ merit function. Several initial guesses were used in order to verify that the minimum $\chi^2$ was not strictly a local minimum. Figure 1 presents an example of the fitting procedure. The frequency-domain $P_1$ model of light transport was fit from 100 to 700 MHz to the imaginary and real parts of the measured PDW in panel (a). Application of Eqs. (2) and (3) transforms these quantities into the more tangible wave amplitude and phase in panel (b).

Instrumentation artifacts such as cable length and source strength variability introduce additional unwanted phase shifts and amplitude decreases. These artifacts may be removed by calibrating the measured PDW phase and amplitude with the phase and amplitude of light detected in a tissue-simulating phantom with known optical properties. Such a calibration scheme is similar in spirit to the lifetime referencing calibration that is routinely performed in frequency-domain fluorescence-lifetime instruments.

Error bars in our results represent the result of many separate measurements and calibrations. In a typical measurement, we measured the tissue several times, and then measured the phantom several times. This procedure provided precision errors that emerge from coupling variability between the probe to the phantom and from the probe to the tissue. The biggest variation in our measurements was due to the variability in coupling to the phantom.

We also made use of some *a priori* information in order to reduce fitting errors. In the NIR it is well known that scattering follows a simple power-law dependence of the form

$$u_s' = A\lambda^{-SP}, \tag{4}$$

where $A$ is a constant and $SP$, the magnitude of the exponent, is the scatter power. Outlier scattering points, as judged arbitrarily by a robust nonlinear fit of $\mu_s'$, were constrained to fit
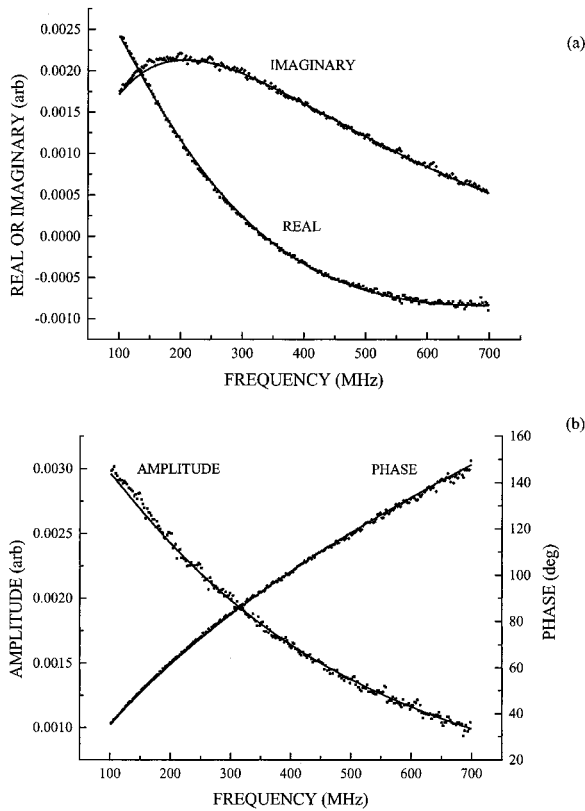
**Fig. 1** *Photon density waves.* (a) Points represent measured real and imaginary parts of the wave, and lines represent a fit of the frequency-domain $P_1$ equation. The result of this fit provides both $\mu_a$ and $\mu_s'$. Note that the real and imaginary parts of this wave are an analog to the amplitude and phase, as described by Eqs. (2) and (3). The direct transformation is provided in panel (b).

the line described by Eq. (4).[46] The real and imaginary components were then refit, while keeping $\mu_s'$ fixed.

## 2.4 Calculation Tissue Physiology: Absorption

Knowledge of the absorption spectrum provides the information needed to solve a weighted least-squares problem to recover the concentrations of the four principal NIR absorbers in tissues: Hb-R, Hb-O$_2$, H$_2$O, and lipids. We assume that other NIR chromophores such as myoglobin are negligible in breast tissue. The term "weighted" refers to weighting the value of $\mu_a$ with its measured error. The least-squares problem expressed as a matrix takes the general form

$$\vec{\mu} = \mathbf{E}\vec{c},\qquad(5)$$

where $\vec{\mu}$ is a vector of length $N$ containing the measured $\mu_a$ values and $\vec{c}$ is a vector of length $M$ containing the chromophore concentrations. The matrix $\mathbf{E}$ has dimensions $N \times M$ and contains the extinction coefficients (cm$^2$ M$^{-1}$) for the $M$ chromophores at each of the $N$ wavelengths. To convert traditional literature molar extinction coefficients (cm$^{-1}$ M$^{-1}$) into extinction coefficients for use in Eq. (5), multiply $\epsilon$ by

$2.303\times10^4$. Since it is difficult to quantify lipids in terms of a concentration, the molar extinction coefficients were used as cm$^2$ Kg$^{-1}$.

The general solution to the matrix problem expressed in Eq. (5) is

$$\vec{c} = (\mathbf{E}^{\mathrm{T}}\mathbf{E})^{-1}\mathbf{E}^{\mathrm{T}}\vec{\mu}\qquad(6)$$

The extinction values for both Hb-R and Hb-O$_2$ were acquired from the work of Wray et al., who used lysed cells in a nonscattering medium.[47] The extinction values for water were interpolated from the work of Hale and Querry.[48] Finally, values for lipids were obtained from Eker, who measured the absorption of soybean oil.[49] We have found using continuous wave spectroscopy that the water spectrum provided by Kou, Labrie, and Chylek provides an overall better spectrum for use in tissue optics studies, although it did not change the essence of our results for the FDPM wavelengths used in this work.[50]

For each measurement we report four hemoglobin parameters: [Hb-R], [Hb-O$_2$], total hemoglobin concentration (*THC*), and the hemoglobin saturation (S$_t$O$_2$), where

$$THC = [\text{Hb}-\text{R}] + [\text{Hb}-\text{O}_2],\qquad(7)$$

$$S_tO_2 = \frac{[\text{Hb}-\text{O}_2]}{[\text{Hb}-\text{R}] + [\text{Hb}-\text{O}_2]}.\qquad(8)$$

Values for water and lipid content are reported as percentages. The water fraction is the concentration of measured tissue water divided by the concentration of pure water (55.6 M). The lipid percentage absorption of lipid measured relative to an assumed "pure" lipid density of 0.9 g mL$^{-1}$. Thus, the reported water and lipid percentages are relative figures of merit compared to pure solutions of the substance, and neither are strict volume nor mass fractions, nor add to 100%.

## 2.5 Measured Tissue Physiology: Scattering

The scattering properties of the tissue also may yield important physiological information. As an example, when the particle size is much smaller than the optical wavelength, *SP* approaches the Rayleigh limit of $-4$. In this work, the magnitude of the slope is referred to as the "scatter power." Intralipid, which is an intravenous fat emulsion that is commonly used as a tissue phantom, has globules of soybean oil that are on average about 97 nm, and yield a value of scatter power of 2.4.[51] Nilsson et al. provided an empirical link between scatter power and the average particle size.[52] This value is not rigorous, but may provide meaningful insight into the origin of the tissue scattering, and ultimately the composition and structure of the breast.

## 2.6 Instrumentation

The specific details of this FDPM instrument has been described in detail elsewhere,[53] but the relevant technical information is mentioned here. The instrument employs seven diode lasers that provided visible and NIR light (672, 800, 806, 852, 896, 913, and 978 nm). A hand-held probe housed an avalanche photodiode (APD) that recorded the modulated diffuse light signals after propagating through the tissue. This

probe has a plastic attachment on the casing to position a source optical fiber 22 mm away from the APD. The optical power launched into the tissue ranged from 5 to 25 mW. A sweep over all seven wavelengths ranged from approximately 35 to 60 s. The system acquired data in less than 3 s per wavelength, with a 2 s delay between each laser diode in the system because of switching considerations. The system was wheeled into a medical clinic for each measurement.

One additional measurement was performed using a steady-state (SS) spectrometer system in conjunction with the FDPM instrument. The technique, known as steady-state FDPM (SSFDPM), has been described in detail elsewhere.[54] In short, the SS system interpolates values of $\mu_a$ between the discrete FDPM measurements. (The NIR scattering spectrum power-law dependence [i.e., Eq. (4)], renders $\mu_s'$ known at all wavelengths of interest. Removing $\mu_s'$ from the problem facilitates the calculation of $\mu_a$ from the steady-state spectrum. See Ref. 54 for details.) The SS system utilizes a separate plastic hand-held probe in which were embedded a source fiber and a detector fiber. The probe fixed the distance between these fibers at 22 mm. Spectra were recorded from 650 to 1000 nm in 2 nm increments, using a 1 s integration time. The system was calibrated using an integrating sphere.

## 2.7 Measurement Procedure

All of the subjects we measured in this study provided informed consent to participate in one of two trials (No. 95-563 and No. 99-2183) that were approved by the Internal Review Board of the University of California at Irvine. All 31 subject ages ranged between 18 and 64. Each subject was in a supine position during the measurement. As outlined above, the instrument probe was the only item placed in contact with the subject. All measurements were performed in a reflection geometry, where we estimate the average depth of penetration was approximately 1 cm below the skin. The probe was placed onto the breast by using the force of gravity as pressure. No compression was used during the measurement. We performed measurements on normal subjects in the center of each of the four quadrants of each breast. Data from the left upper outer quadrant are presented here, although the data presented here are representative of other sites.

One SSFDPM measurement was also performed upon a 37-year-old woman with a lesion located in the upper inner quadrant of her left breast [Figure 2(a)]. The subject was postmenopausal surgically since age 28. Prior fine-needle aspiration confirmed the lesion to be a fibroadenoma. The lesion dimensions were determined by conventional clinical ultrasound at the time of the SSFDPM measurement to be approximately 19 by 19 by 10 mm at a depth of 11 mm below the skin. SSFDPM measurements were performed at seven discrete positions in a line on the skin [Figure 2(b)]. FDPM measurements were first performed along the seven points, and then followed by SS measurements at the same locations. This process was repeated for the same location on the healthy breast. Only the line scan from medial to lateral is presented here.
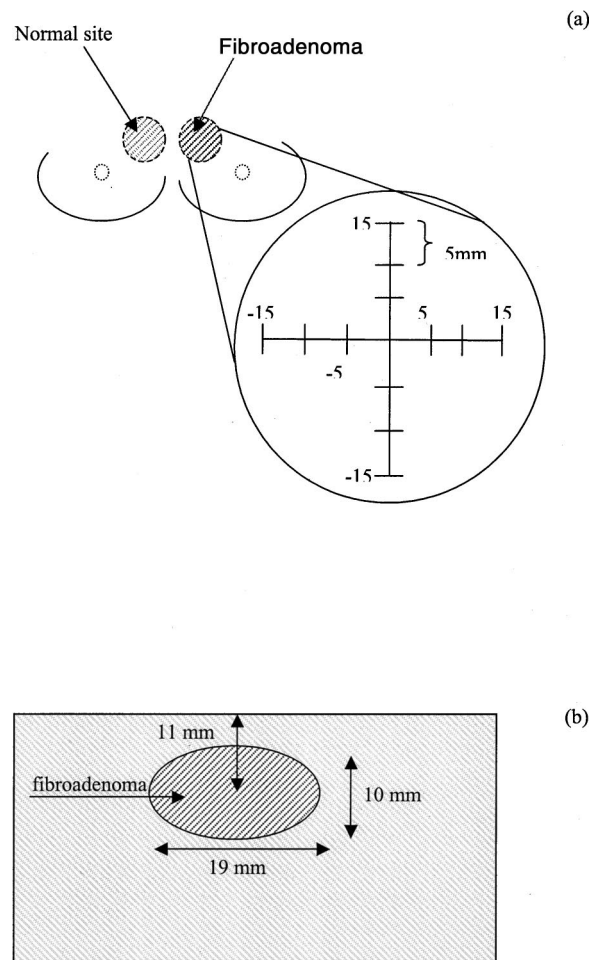
**Fig. 2** *SSFDPM measurement locations.* Panel (a) displays the measurement grid for placement of the probes. The site of the fibroadenoma was determined via standard clinical ultrasound. Panel (b) indicates the dimensions of the fibroadenoma. The axis of the lesion into the page was also 19 mm.

## 3 Results

### 3.1 Measurement of Water and Lipids *In Vivo*

Age-dependent changes in water and lipid fractions are presented in Figures 3 and 4, respectively. Premenopausal subjects (i.e., age <50) display a variety of values. Inter-subject variations include, but are not limited to, menstrual cycle differences and gynecological age. The same general trend occurs in the *THC*.[15] The water seems to increase in premenopausal subjects (ages 18–39), perhaps reaching a peak value near the age of 30. Between the ages of 40–49, water seems to decline. After age 50 (predominantly postmenopausal) there is a general decrease with age in water, and an increase in lipids. Error bars represent the results of repeated measurements. The late decrease in *THC* and water correlates well the atrophy of well-vascularized lobular tissue and the increase of the fat-to-collagen ratio after menopause.[14] Compositional analysis data show lower blood and water content for fat versus glandular tissue.[55]

Measured lipid and scatter power are presented as functions of body-mass index (BMI) in Figures 5 and 6, respec-
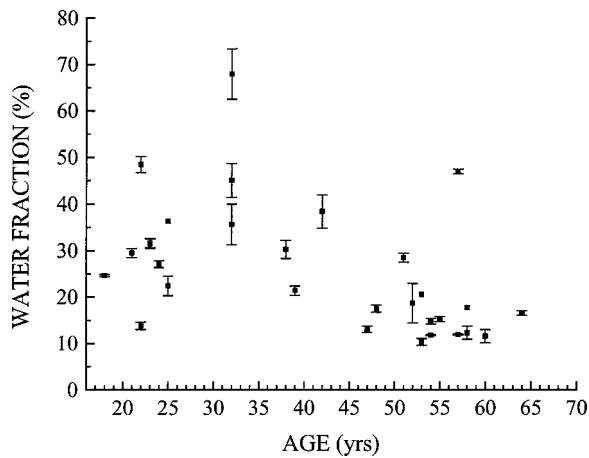
**Fig. 3** *Water vs age.* The water fraction is the water concentration in tissue relative to the concentration of pure water (55.6 M). Premenopausal volunteers (<age 50) show considerable variation over age because of intra-subject variations such as menstrual cycle variations and overall hormone production differences. Postmenopausal and peri-menopausal (>age 50) volunteers appear to show a decrease in water content.



**Fig. 5** *Lipid fraction and BMI.* A general check of our ability to measure lipids in breast tissue is to scale them against BMI. Women within a single BMI unit were averaged together to form the histogram. This is a general (not absolute) trend that we would expect to find in breast.

tively. The BMI scale is determined by dividing body mass (Kg) by height squared ($m^2$), and numbers between 20 and 25 are considered normal.[56] The histograms represent an average over all BMI values within a single BMI unit. The error bars represent the subject variation within a given BMI bin. There is a general correlation between lipid mass density with BMI. Overall body mass and breast mass are not perfectly correlated, so that this correlation is not expected to be perfect. Collagen-rich glandular tissue scatters light with a higher scatter power than adipose tissue.[57] Thus, smaller scatter powers are expected in fatty tissue. In the postmenopausal breast the ratio of adipose to glandular tissue generally decreases, which should result in a lower scatter power. Such an interpretation may not be valid given that the amount of collagen in each breast is not known. However, it should be empha-
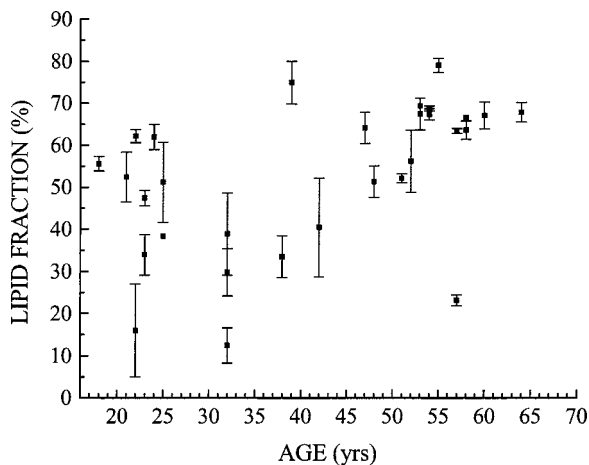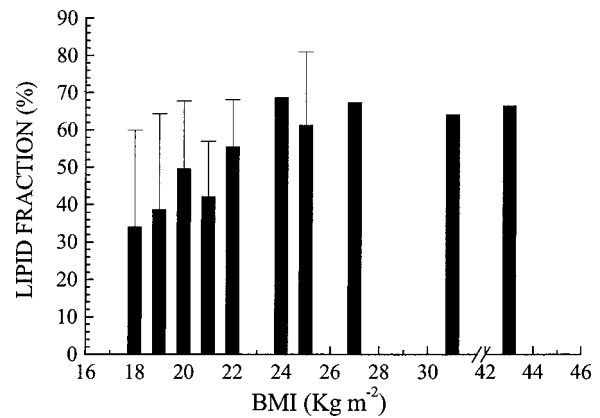
sized that the scattering and the absorption information together provide a consistent picture of the components in the breast.

## 3.2 Spectral Content in Scattering

Figures 7 and 8 further support the idea that tissue scattering spectra provide important physiological content. In Figure 7, the measured scattering at 800 nm does display a clear pattern that may provide any significant information content. The scattering spectral dependence, however, tells a different story. Figure 8 clearly demonstrates that the scattering spectrum (i.e., scatter power), shows a marked decrease as a function of age. Again, we expect that breasts full of highly scattering, collagen-rich tissue would display a higher scatter power than breasts with more adipose.

## 3.3 Effect of Water and Lipids in Breast

All of the previous figures demonstrate the highly variable, but physiologically intuitive, amounts of water, lipids, and scattering found in normal breast tissue. The next two figures demonstrate how neglecting an individual's water and
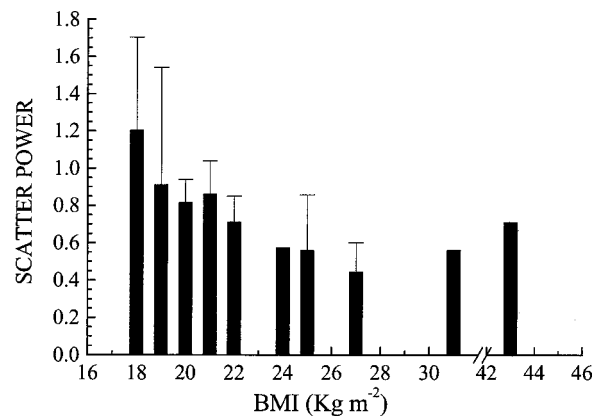


**Fig. 4** *Lipids vs age.* The lipid fraction is the lipid mass density (g mL$^{-1}$) in tissue relative to a lipid mass density of 0.9 g mL$^{-1}$. Again, variations exist, although there is a general increasing trend with age.



**Fig. 6** *Scatter power and BMI.* Complementary information is provided by the scattering properties of the tissue. Women within a single BMI unit were averaged together to form the histogram. Note that we would expect in general a lower scatter power in fattier tissue.
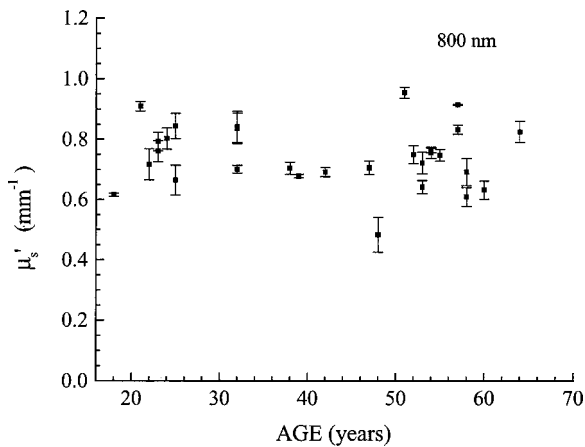
**Fig. 7** *Scattering in breast at 800 nm.* These points represent the average measured $\mu_s'$ values in 29 healthy volunteers as a function of age. No obvious distinctive pattern emerges.

lipid content affects measurements of breast *THC* and $S_tO_2$. The following calculations represent the percent deviation between the "true" values and the values one would measure using only $\mu_a$ at 672, 806, and 849 nm, three abovementioned wavelengths; note that the "abs %" refers to an absolute change in $S_tO_2$, i.e., 80%–85%. Panels (a) and (b) present the *THC* and $S_tO_2$, respectively, of a pre-menopausal breast, assuming that $THC = 27.4 \mu M$ and $S_tO_2 = 76.6\%$. Panels (c) and (d) provide the same information, but for a postmenopausal breast using $THC = 14.6 \mu M$ and $S_tO_2 = 82.2\%$. (These average values are based upon averages measured in our trial). Figure 9 ignores entirely the contribution of water and lipids, whereas Figure 10 assumes a background value of water and lipids, using 33% and 44% for the pre-menopausal breast in (a) and (b), and 19% and 61% for the post-menopausal breast in (c) and (d), respectively.

Figure 9 readily displays that serious errors may result by ignoring contributions from water and lipids. Values of water



**Fig. 8** *Scatter power in breast.* The effect of the spectrum of the tissue scattering is more clearly demonstrated. Scatter power is the exponent of the scattering vs wavelength dependence, as shown in Eq. (4). This time, there is a distinctive general decrease with age, which is not obvious at any single wavelength. This general pattern is also true of mammographic density.

are provided over a wide range for three different lipid fractions; the three lines represent lipid fractions of 20%, 45%, and 70%, in ascending order. Water is highly variable in breast, leading from anywhere between 10% and 30% over-estimation of *THC* [panel (a)] and 2%–6% rise in $S_tO_2$ [panel (b)]. The effect is even more pronounced in the postmenopausal case [panels (c) and (d)], where the error in *THC* and $S_tO_2$ jump to higher errors.

Figure 10, which assumes reasonable background water and lipid values reflective of our measurements in both pre- and postmenopausal cases, has some definite improvements. Of course, if the true water and lipid content is close to the assumed background value, the error is small. The effect of the background is to shift the error curves from always positive, to both positive and negative estimations of *THC* and $S_tO_2$. The errors may be significant if the assumed value differs significantly from the true value.

## 3.4 Fibroadenoma as an Example

Figures 11 and 12 display the results of SSFDPM measurements performed over regions of normal and diseased tissue. In both figures, triangles represent measurements performed on or near the site of the fibroadenoma, whereas the squares represent measurements performed on the healthy breast in the same anatomical site as the fibroadenoma. The *THC* in Figure 11 is higher over the fibroadenoma, and slightly decreased relative to normal outside the lateral extent of the lesion. Figure 12 provides a more convincing case, but this time in water fraction. Although not shown, the lipid fraction takes a similar course, though to a lesser extent; the lipid fraction on the fibroadenoma was about 5% lower than over normal tissue. Equally important is the fact that $S_tO_2$ (i.e., Figure 13) decreases only slightly over the fibroadenoma site, and may not provide enough contrast by itself for detection. Interestingly, the largest decreases in $S_tO_2$ occur near the fibroadenoma boundaries.

## 4 Discussion

### 4.1 Spectroscopy is the Key

The results presented in this work strongly suggest that the spectral signature of diffuse optical signals provides distinctive functional information in the breast. It is not surprising that the pre- and postmenopausal breast display the physiological trends that we have observed. Regardless, it should be stressed that we have been able to quantify these functional changes noninvasively.

A single wavelength of light may be used to detect some breast lesions, but it will not compete with the spatial resolution offered by conventional techniques. However, by providing spectroscopic information about a suspicious region of tissue, optics may prove useful in the management of breast disease. Note that the advantages of spectroscopy are not solely restricted to measurements of $\mu_a$; the spectral dependence of $\mu_s'$ also contains important information. Tissue absorption and scattering information together appear to paint a more complete picture of the tissue composition than direct measurements of optical attenuation.
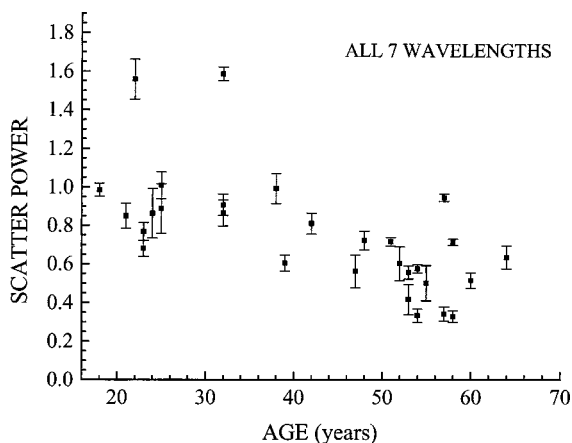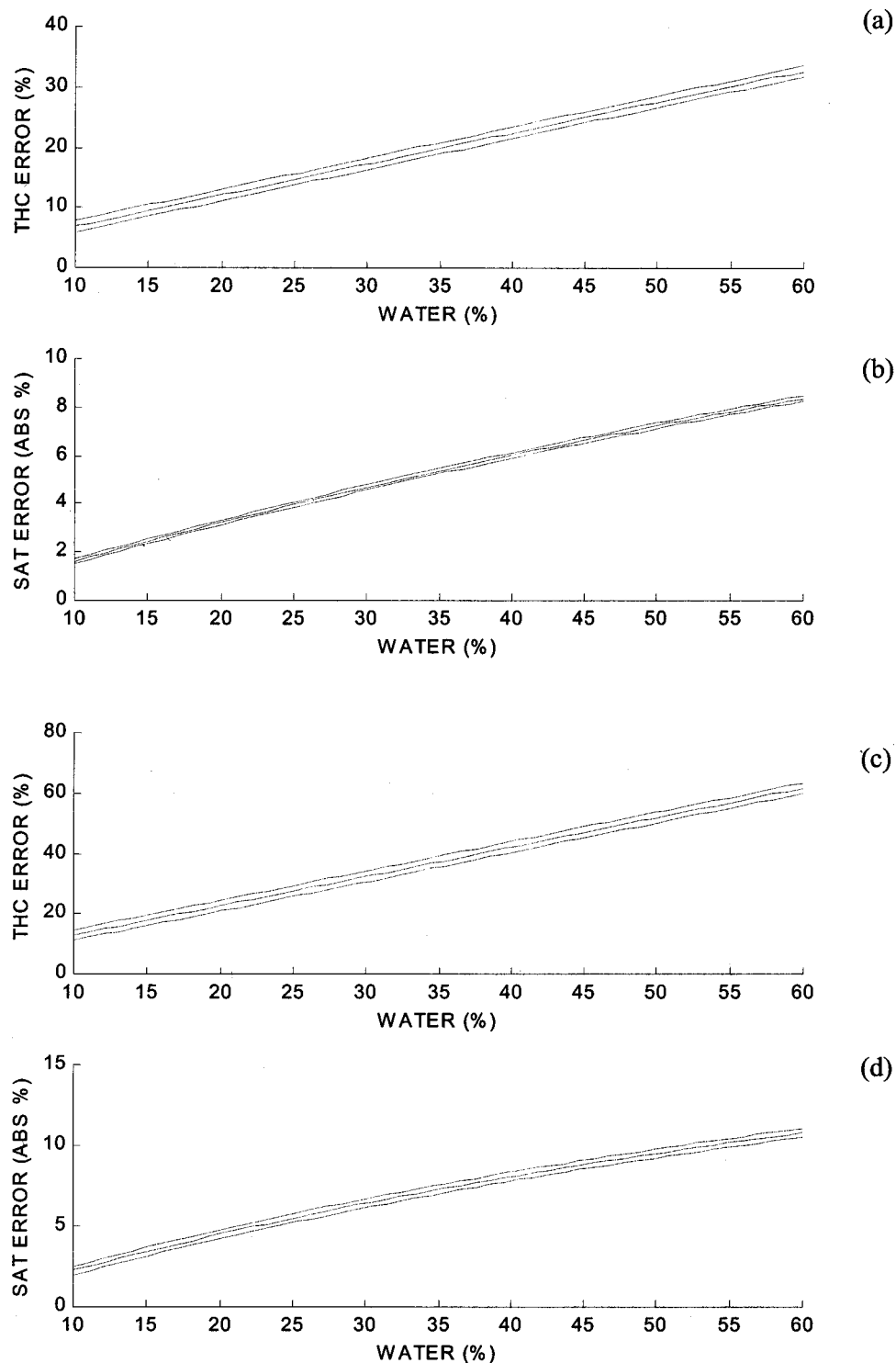
**Fig. 9** *Effects of ignoring water and lipids.* Panels (a) and (b) represent a pre-menopausal woman with $THC = 27.4 \, \mu M$ and $S_tO_2 = 76.6\%$. Panels (c) and (d) provide the same information, but for a postmenopausal breast using $THC = 14.6 \, \mu M$ and $S_tO_2 = 82.2\%$. The percent errors are determined by calculating the $THC$ and $S_tO_2$ perceived by using only absorption values at 672, 806, and 849 nm and comparing them to the true values listed above. The three lines represent values of 20%, 45%, and 70% lipids in the calculation, in ascending order.

We have demonstrated that our measurements at seven discrete wavelengths seem enough to account for the blood, water, and lipid content of breast. Instruments restricted to two or three wavelengths sacrifice important spectroscopic informa-tion. It is fortunate that two of the diodes, namely at 913 and 978 nm, lie very close to the absorption peaks of lipids and water, respectively. The SSFDPM technique adds tremendous spectral bandwidth to a discrete wavelength measurement, but
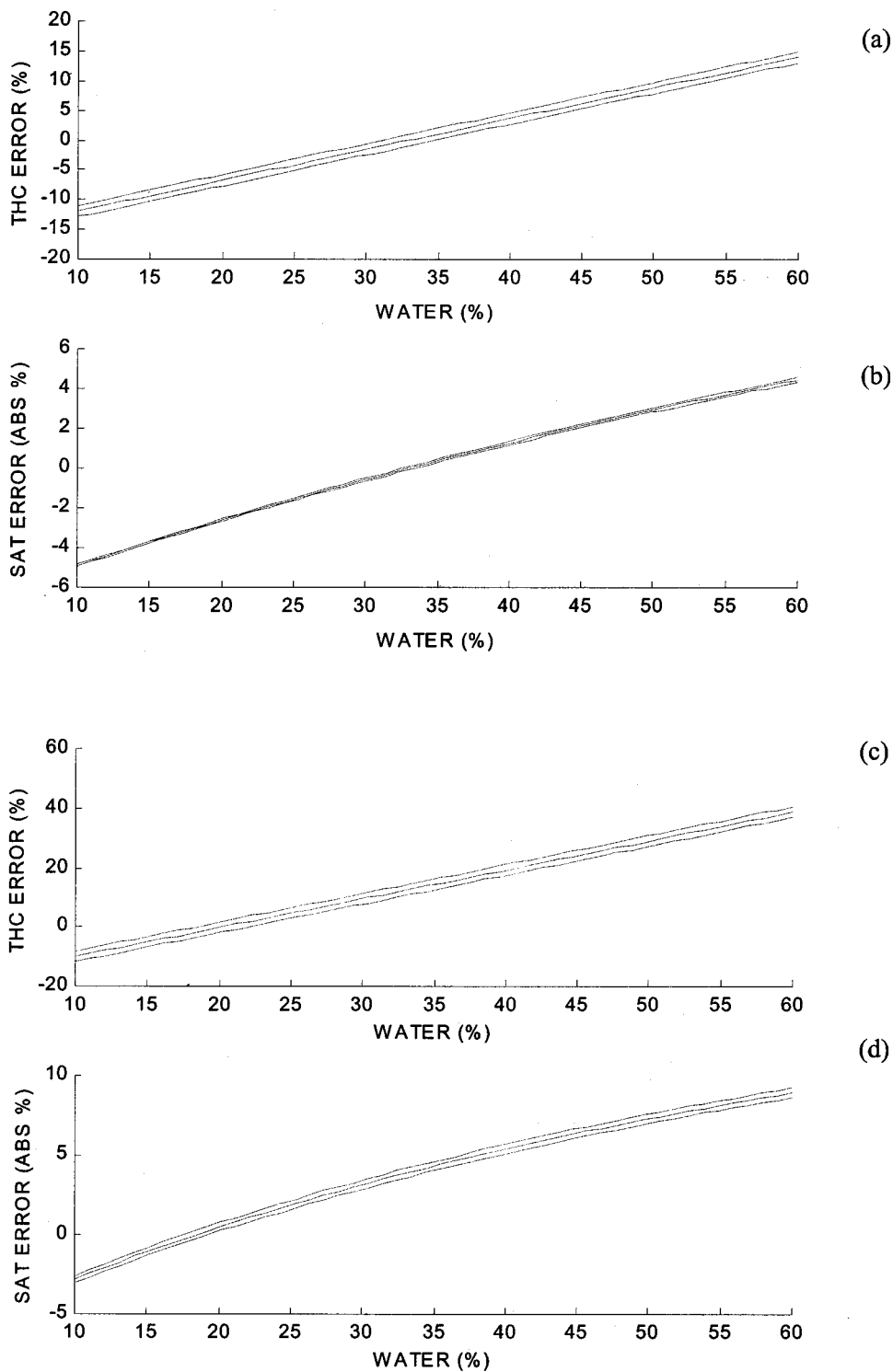
**Fig. 10** *Effects of assuming water and lipid values.* Same description as Figure 9, but this time assuming water and lipid fractions of 33% and 44% for the pre-menopausal breast [panels (a) and (b)], and 19% and 61% for the postmenopausal breast [panels (c) and (d)], respectively.

it is still reliant upon discrete measurements of $\mu_s'$. The topic of determining the optimal selection of wavelengths is currently under investigation.

## 4.2 Normal Optical Properties Needed

Ignoring the contributions of water and lipids in the breast leads to errors in the measurement of *THC* and $S_tO_2$. Earlier work has also suggested that ignoring water in NIR measurements will lead to significant errors in some conditions. Franceschini et al. asserted that knowledge of the water concentration was required in order to determine accurately the $S_tO_2$ of 23 $\mu$M of blood suspended in a scattering medium using a two wavelength technique (715 and 825 nm).[58] Hemoglobin concentrations in adult muscle can easily be on the
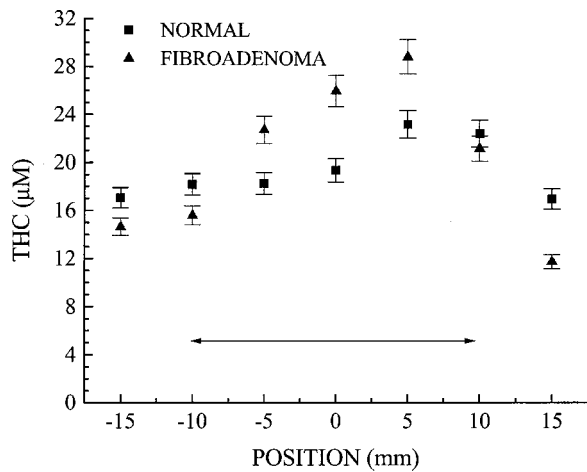
**Fig. 11** *THC in a fibroadenoma.* SSFDPM measurements of a fibroadenoma (triangles) vs-same-site normal tissue on the opposite breast (squares) in a 37-year-old postmenopausal woman. Measurements spanned the region from 650 to 1000 nm, using a four-component fit as described above. The fibroadenoma covers the region between approximately −10 to +10 mm (as indicated by the bar), where there is a general increase in *THC*. Although the fibroadenoma is "visible," would this be enough information to distinguish it from other lesions or breast components?

order of 100 $\mu$M as determined by deep-tissue measurements in a reflection geometry. Neglecting water in high Hb concentration environments translates into errors less than 5% in $S_tO_2$ for values above 50%.[58] However, the breast is a totally different matter. The overall measured concentrations of Hb are much lower in breast than in muscle. Hull, Nichols, and Foster point out clearly that two or three wavelength systems can produce significant errors as well, although their three wavelength system did not include a water peak.[59] Thus, it is not just the number of wavelengths, but also the sensitivity of those wavelengths to selected chromophores that are important in discrete wavelength measurements. Adding wavelengths more sensitive to water (such as 980 nm) can help quantify the water concentration. The SSFDPM technique adds even more bandwidth.
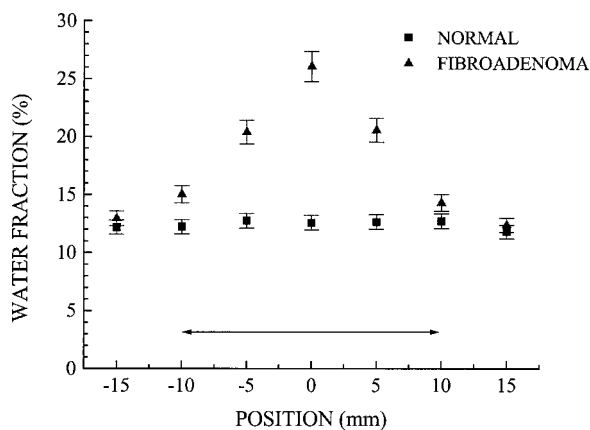


**Fig. 12** *Water concentration in a fibroadenoma.* The details of this figure are the same as for Figure 11, except water is plotted instead of *THC*. Notice the high contrast available from water.
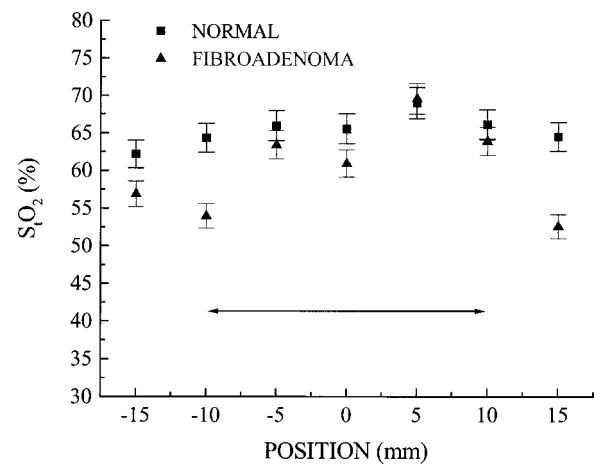


**Fig. 13** $S_tO_2$ *in a fibroadenoma.* The details of this figure are the same as for the previous two figures. A minor decrease in $S_tO_2$ over the fibroadenoma is noticeable.

### 4.3 Necessity of Control Values

In general, pre-menopausal breast is more optically attenuating than postmenopausal breast, both in absorption and scattering. It is important to note that this trend, particularly in scatter power, is also true for mammographic density. The balance between fat, collagen, epithelium, and water is responsible for changes in mammographic density.[60] Our measurements suggest that the collagen to lipid ratio strongly influences NIR optical scattering. NIR spectroscopy has unique potential for quantifying the specific elements of breast tissue that contribute to mammographic density. This observation may be of importance in risk assessment, since mammographic density has been cited as a risk for breast cancer.[60] Thus, optical methods may identify breast tissue at physiological risk for malignant transformation and can be performed easily in all women at any age.

Knowledge of the normal values of NIR chromophores will play an important role in evaluating the usefulness of optical methods in detecting and characterizing lesions in the breast. Several investigators have reported a two-to-fourfold *THC* contrast between normal and tumor structures; *in vivo* tumor $S_tO_2$ values are also typically lower than normal tissue.[29–31] Neglecting the effects of water and lipids further complicates efforts for accurate quantitative diagnosis. The effect of falsely ascribing lipid and water absorption to hemoglobin will inflate measured values of Hb-O$_2$, and thus inflate measurements of *THC* and $S_tO_2$. This change in contrast will decrease the probability for success of noninvasive optical lesion characterization. For every woman, the effect of water and lipids will vary so that the error in measured hemoglobin levels will be different, and potentially unpredictable. The effect will be more severe for patients with lower *THC* levels, i.e., older women. There is also no reason to assume that the distribution of water and lipids will be uniform across the whole breast.

Detailed studies of normal tissue are essential for determining the sensitivity required of optical instrumentation for detecting lesions in women of varying age and hormonal status. As base line levels are characterized, data on an individual's absorption and scattering variations could provide impor-

tant insight into disease appearance and progression. When applied to patients receiving chemotherapy and/or hormone replacement therapies, this information could also be used to generate feedback that would permit customized treatment planning based upon individual physiologic response. Experiments such as these are currently under way.

## 4.4 Additional Comments

For the case of fibroadenoma versus normal the water content differences were substantial. This is in part due to the low postmenopausal water concentrations; such contrast may not be present in the case of a pre-menopausal subject. $THC$ and $S_tO_2$ alone may not provide enough unique information to adequately distinguish benign lesions such as fibroadenoma from malignant ones. A combination of hemodynamic information with the water and lipid content may be necessary for the successful NIR classification of breast lesions. More subjects will be needed to establish this conjecture.

One potential problem with our analysis of the 30 normal subjects is the absorption overlap between lipids and water. Seven wavelengths may not provide enough spectral resolution to quantify these two chromophores independently. We have shown in another work that the water and lipid absorption information parallels information obtained from the scatter power.[15] Thus, we do not expect this cross talk to affect the general trends we have observed in our normal subjects. The SSFDPM technique has a much wider spectral bandwidth, which minimizes these cross talk problems. We now use an integrated SSFDPM system in all our measurements.

## 5 Conclusions

Multi-spectral measurements provide distinct advantages over two or three wavelength measurements. Although a large *number* of wavelengths may enhance sensitivity to hemoglobin, a large spectral *range* is also important. In addition, the reliability of water and lipids measurements improves substantially when spectral information beyond approximately 830 nm is included.

The water and lipid levels in normal breast vary significantly with age and hormonal status, particularly between pre- and postmenopausal subjects. Ignoring water and lipid absorption can produce artificially high $THC$ and $S_tO_2$ values of perhaps 20%–30% and 5%, respectively. These errors will be different for each individual patient. Tissue scattering may also prove to be a useful diagnostic parameter. Our results show that the spectral dependence of scattering can provide key insights into breast composition and physiology, whereas scattering at a single wavelength may not. Overall, the wealth of additional information provided by broadband, multi-spectral measurements appears to be a key step towards improving accuracy in optical breast diagnostics.

## References

1. M. Cutler, "Transillumination as an aid in the diagnosis of breast lesions," *Surg. Gynecol. Obstet.* **48**, 721–728 (1929).
2. E. Carlsen, *Diagnostic Imaging*, Spectrascan, S. Windsor, CT (1982).
3. R. J. Bartrum, Jr. and H. C. Crow, "Transillumination lightscanning to diagnose breast cancer: A feasibility study," *AJR, Am. J. Roentgenol.* **142**(2), 409–414 (1984).
4. H. Wallberg, A. Alveryd, U. Bergvall, K. Nasiell, P. Sundelin, and S. Troell, "Diaphanography in breast carcinoma. Correlation with clinical examination, mammography, cytology and histology," *Acta Radiol.: Diagn.* **26**(1), 33–44 (1985).
5. N. Bundred, P. Levack, D. J. Watmough, and J. A. Watmough, "Preliminary results using computerized telediaphanography for investigating breast disease," *Br. J. Hosp. Med.* **37**(1), 70–71 (1987).
6. B. Drexler, J. L. Davis, and G. Schofield, "Diaphanography in the diagnosis of breast cancer," *Radiology* **157**(1), 41–44 (1985).
7. B. Monsees, J. M. Destouet, and D. Gersell, "Light scanning of nonpalpable breast lesions: Reevaluation," *Radiology* **167**(2), 352 (1988).
8. A. Alveryd, I. Andersson, K. Aspegren, G. Balldin, N. Bjurstam, G. Edström, G. Fagerberg, U. Glas, O. Jarlman, and S. A. Larsson et al., "Lightscanning versus mammography for the detection of breast cancer in screening and clinical practice. A Swedish multicenter study," *Cancer* **65**(8), 1671–1677 (1990).
9. A. H. Gandjbakhche, R. Nossal, and R. F. Bonner, "Resolution limits for optical transillumination of abnormalities deeply embedded in tissues," *Med. Phys.* **21**(2), 185–191 (1994).
10. E. M. Sevick, B. Change, J. Leigh, S. Nioka, and M. Maris, "Quantitation of time-resolved and frequency-resolved optical spectra for the determination of tissue oxygenation," *Anal. Biochem.* **195**(2), 330–351 (1991).
11. S. Ertefai and A. E. Profio, "Spectral transmittance and contrast in breast diaphanography," *Med. Phys.* **12**(4), 393–400 (1985).
12. V. Quaresima, S. J. Matcher, and M. Ferrari, "Identification and quantification of intrinsic optical contrast for near-infrared mammography," *Photochem. Photobiol.* **67**(1), 4–14 (1998).
13. R. Cubeddu, C. D. Andrea, A. Pifferi, P. Taroni, A. Torricelli, and G. Valentini, "Effects of the menstrual cycle on the red and near-infrared optical properties of the human breast," *Photochem. Photobiol.* **72**(3), 383–391 (2000).
14. S. Thomsen and D. Tatman, "Physiological and pathological factors of human breast disease that can influence optical diagnosis," *Ann. N.Y. Acad. Sci.* **838**, 171–193 (1998).
15. A. E. Cerussi, A. J. Berger, F. Bevilacqua, N. Shah, D. Jakubowski, J. Butler, R. F. Holcombe, and B. J. Tromberg, "Sources of absorption and scattering contrast for non-invasive optical mammography," *Acad. Radiol.* **8**, 211–218 (2001).
16. S. L. Jacques, "Origins of tissue optical properties in the UVA, Visible, and NIR Regions," OSA TOPS: Advances in Optical Imaging and Photon Migration, R.R. Alfano and J. G. Fujimoto, Eds., **2**, 364–371, Optical Society of America, Washington (1996).
17. S. J. Matcher, M. Cope, and D. T. Delpy, "*In vivo* measurements of the wavelength dependence of tissue-scattering coefficients between 760 and 900 nm measured with time-resolved spectroscopy," *Appl. Opt.* **36**(1), 386–396 (1997).
18. J. R. Mourant, M. Canpolat, C. Brocker, O. Esponda-Ramos, T. M. Johnson, A. Matanock, K. Stetter, and J. P. Freyer, "Light scattering from cells: the contribution of the nucleus and the effects of proliferative stats," *J. Biomed Opt.* **5**(2), 131–137 (2000).
19. B. J. Tromberg, N. Shah, R. Lanning, A. Cerussi, J. Espinoza, T. Pham, L. Svaasand, and J. Butler, "Non-invasive in vivo characterization of breast tumors using photon migration spectroscopy," *Neoplasia* **2**(1), 1–15 (2000).
20. R. Hornung, T. H. Pham, K. A. Keefe, M. W. Berns, Y. Tadir, and B.

J. Tromberg, "Quantitative near-infrared spectroscopy of cervical dysplasia in vivo," *Hum. Reprod.* **14**(11), 2908–2916 (1999).

21. D. J. Watmough, "Diaphanography. Mechanism responsible for the images," *Acta Radiol.* **21**(1), 11–15 (1982).

22. A. E. Profio, G. A. Navarro, and O. W. Sartorius, "Scientific basis of breast diaphanography," *Med. Phys.* **16**(1), 60–65 (1989).

23. M. S. Patterson, B. Chance, and B. C. Wilson, "Time resolved reflectance and transmittance for the non-invasive measurement of tissue optical properties," *Appl. Opt.* **28**(12), 2331–2336 (1989).

24. J. B. Fishkin and E. Gratton, "Propagation of photon-density waves in strongly scattering media containing an absorbing semi-infinite plane bounded by a straight edge," *J. Opt. Soc. Am. A* **10**(1), 127–140 (1993).

25. S. Andersson-Engels, R. Berg, and S. Svanberg, "Effects of optical constants on time-gated transillumination of tissue and tissue-like media," *J. Photochem. Photobiol., B* **16**(2), 155–167 (1992).

26. S. B. Colak, M. B. van der Mark, G. W.'t Hooft, J. H. Hoogenraad, E. S. van der Linden, and F. A. Kuijpers, "Clinical optical tomography and NIR spectroscopy for breast cancer detection," *IEEE J. Sel. Top. Quantum Electron.* **5**(4), 1143–1158 (1999).

27. R. J. Grable, D. P. Rohler, and S. Kla, "Optical tomography breast imaging," in Optical Tomography and Spectroscopy of Tissue: Theory, Instrumentation, Model, and Human Studies II, B. Chance and R. R. Allfano, Eds., Vol. 2979, pp. 197-210, SPIE, Bellingham (1997).

28. M. A. Franceschini, K. T. Moesta, S. Fantini, G. Gaida, E. Gratton, H. Jess, W. W. Mantulin, M. Seeber, P. M. Schlag, and M. Kaschke, "Frequency-domain techniques enhance optical mammography: Initial clinical results," *Proc. Natl. Acad. Sci. U.S.A.* **94**(12), 6468–6473 (1997).

29. J. B. Fishkin, O. Coquoz, E. R. Anderson, M. Brenner, and B. J. Tromberg, "Frequency-domain photon migration measurements of normal and malignant tissue optical properties in a human subject," *Appl. Opt.* **36**(1), 10–20 (1997).

30. S. Fantini, S. A. Walker, M. A. Franceschini, M. Kaschke, P. M. Schlag, and K. T. Moesta, "Assessment of the size, position, and optical properties of breast tumors in vivo by noninvasive optical methods," *Appl. Opt.* **37**(10), 1982–1989 (1998).

31. T. O. McBride, B. W. Pogue, E. D. Gerety, S. B. Poplack, U. L. Osterberg, and K. D. Paulsen, "Spectroscopic diffuse optical tomography for the quantitative assessment of hemoglobin concentration and oxygen saturation in breast tissue," *Appl. Opt.* **38**(25), 5480–5490 (1999).

32. D. Grosenick, H. Wabnitz, H. H. Rinneberg, K. T. Moesta, and P. M. Schlag, "Development of a time-domain optical mammograph and first in vivo applications," *Appl. Opt.* **38**(13), 2927–2943 (1999).

33. O. Jarlman, R. Berg, S. Andersson-Engels, S. Svanberg, and H. Pettersson, "Time-resolved white light transillumination for optical imaging," *Acta Radiol.* **38**(1), 185–189 (1997).

34. K. A. Kang, B. Chance, S. Zhao, S. Srinivasan, E. Patterson, and R. Troupin, "Breast tumor characterization using near infrared spectroscopy," in Photon Migration and Imaging in Random Media and Tissues, B. Chance and R. R. Alfano, Eds., Vol. 1888, pp. 487–499, SPIE, Bellingham (1993).

35. K. Suzuki, Y. Yamashita, K. Ohta, and B. Chance, "Quantitative measurement of optical parameters in the breast using time-resolved spectroscopy. Phantom and preliminary in vivo results," *Invest. Radiol.* **29**(4), 410–414 (1994).

36. K. Suzuki, Y. Yamashita, K. Ohta, M. Kaneko, M. Yoshida, and B. Chance, "Quantitative measurement of optical parameters in normal breasts using time-resolved spectroscopy: In vivo results of 30 Japanese women," *J. Biomed. Opt.* **1**(3), 330–334 (1996).

37. H. Heusmann, J. Kölzer, and G. Mitic, "Characterization of female breasts in vivo by time-resolved and spectroscopic measurements in near infrared spectroscopy," *J. Biomed. Opt.* **1**, 425–434 (1996).

38. J. Brisson, A. S. Morrison, and N. Khalid, "Mammographic parenchymal features and breast cancer in the Breast Cancer Detection Demonstration Project," *J. Natl. Cancer Inst.* **80**(19), 1534–1540 (1988).

39. N. F. Boyd, C. Greenberg, G. Lockwood, L. Little, L. Martin, J. Byng, M. Yaffe, and D. Tritchler, "Effects at two years of a low-fat, high-carbohydrate diet on radiologic features of the breast: Results from a randomized trial," *J. Natl. Cancer Inst.* **89**(7), 488–496 (1997).

40. N. A. Lee, H. Rusinek, J. Weinreb, R. Chandra, H. Toth, C. Singer, and G. Newstead, "Fatty and fibroglandular tissue volumes in the breasts of women 20–83 years old: Comparison of X-ray mammography and computer-assisted MR imaging (see comments)," *AJR, Am. J. Roentgenol.* **168**(2), 501–506 (1997).

41. L. O. Svaasand, B. J. Tromberg, R. C. Haskell, T. Tsong-Tseh, and M. W. Berns, "Tissue characterization and imaging using photon density waves," *Opt. Eng.* **32**(2), 258–266 (1993).

42. J. B. Fishkin, S. Fantini, M. J. vande Ven, and E. Gratton, "Gigahertz photon density waves in a turbid medium: Theory and experiments," *Phys. Rev. E* **53**(3), 2307–2319 (1996).

43. J. M. Kaltenbach and M. Kaschke, "Frequency- and time-domain modeling of light transport in random media," in *Medical Optical Tomography: Functional Imaging and Monitoring*, G. Müller, B. Chance, R. Alfano, S. Arridge, J. Beuthan, E. Gratton, M. Kaschke, B. Masters, S. Svanberg, P. v. d. Zee, and R. F. Potter, Eds., Vol. IS11, pp. 65–86, Society of Photo-Optical Instrumentation Engineers, Bellingham (1993).

44. R. A. J. Groenhuis, H. A. Ferwerda, and J. J. Ten Bosch, "Scattering and absorption of turbid materials determined from reflection measurements. I. Theory," *Appl. Opt.* **22**(16), 2456–2462 (1983).

45. F. P. Bolin, L. E. Preuss, R. C. Taylor, and R. J. Ference, "Refractive index of some mammalian tissues using a fiber optic cladding method," *Appl. Opt.* **28**(12), 2297–2303 (1989).

46. W. H. Press, S. A. Teukolsky, W. T. Vetterling, and B. P. Flannery, *Numerical Recipies in C*, 2nd ed., Cambridge University Press, Cambridge, UK (1992).

47. S. Wray, M. Cope, D. T. Delpy, J. S. Wyatt, and E. O. Reynolds, "Characterization of the near infrared absorption spectra of cytochrome aa3 and haemoglobin for the non-invasive monitoring of cerebral oxygenation," *Biochim. Biophys. Acta* **933**(1), 184–192 (1988).

48. G. M. Hale and M. R. Querry, "Optical constants of water in the 200 nm to 200 mu m wavelength region," *Appl. Opt.* **12**(3), 555–563 (1973).

49. C. Eker, "Optical characterization of tissue for medical diagnostics," PhD thesis, Lund Institute of Technology (1999).

50. L. Kou, D. Labrie, and P. Chylek, "Refractive indices of water and ice in the 0.65–2.5 mu m spectral range," *Appl. Opt.* **32**(19), 3531–3540 (1993).

51. H. J. van Staveren, C. J. M. Moes, J. van Marle, S. A. Prahl, and M. J. C. van Gemert, "Light scattering in Intralipid-10% in the wavelength range of 400–1100 nm," *Appl. Opt.* **30**(31), 4507–4514 (1991).

52. A. M. K. Nilsson, C. Sturesson, D. L. Liu, and S. Andersson-Engels, "Changes in spectral shape of tissue optical properties in conjunction with laser-induced thermotherapy," *Appl. Opt.* **37**(7), 1256–1267 (1998).

53. T. Pham, O. Coquoz, J. Fishkin, E. A. Anderson, and B. J. Tromberg, "A broad bandwidth frequency domain instrument for quantitative tissue optical spectroscopy," *Rev. Sci. Instrum.* **71**(6), 1–14 (2000).

54. F. Bevilacqua, A. J. Berger, A. E. Cerussi, D. Jakubowski, and B. J. Tromberg, "Broadband absorption spectroscopy in turbid media by combined frequency-domain and steady-state methods," *Appl. Opt.* **39**(34), 6498–6507 (2000).

55. F. A. Duck, *Physical Properties of Tissue*, pp. 319–328, Academic, London (1990).

56. *Merck Manual*, M. Beers and R. Berkow, Eds., p. 14, Merck Research Laboratories, Whitehouse Station, NJ (1999).

57. V. G. Peters, D. R. Wyman, M. S. Patterson, and G. L. Frank, "Optical properties of normal and diseased human breast tissues in the visible and near infrared," *Phys. Med. Biol.* **35**(9), 1317–1334 (1990).

58. M. A. Franceschini, S. Fantini, A. Cerussi, B. Barbieri, B. Chance, and E. Gratton, "Quantitative spectroscopic determination of hemoglobin concentration and saturation in a turbid medium: Analysis of the effect of water absorption," *J. Biomed. Opt.* **2**(2), 147–153 (1997).

59. E. L. Hull, M. G. Nichols, and T. H. Foster, "Quantitative broadband near-infrared spectroscopy of tissue-simulating phantoms containing erythrocytes," *Phys. Med. Biol.* **43**(11), 3381–3404 (1998).

60. A. M. Oza and N. F. Boyd, "Mammographic parenchymal patterns: A marker of breast cancer risk," *Epidemiol. Rev.* **15**(1), 196–208 (1993).